JCRMHS
Journal of Clinical Case Reports, Medical Images and Health Sciences
Volume 8 Issue 4, 2024
Article Information
Received date: 25/11/2024
Published date: 05/12/2024

*Corresponding author
*Cristiane Wenceslau Valverde, Laboratory of Genetics, Butantan Institute, Av. Vital Brazil 1500, ZIP 05503-900, São Paulo, SP, Brazil.

*Key Words:
Biodistribution; Human immature dental pulp cells; Cell therapy product; Bioluminescence image (BLI); Inductively coupled plasma mass spectrometer (ICP-MS)

Research Article

Assessing the Biodistribution of Human Immature Dental Pulp Stem Cells (NestaCell®) via Intravenous Administration in Mice: A Non-Clinical Investigation

Cristiane Wenceslau Valverde[1]*, Vivian Fonseca Gonzaga[2], Bruna de Oliveira Policiquio[2], Leandro Hideki Ynoue[3], Luciana Ferrara[3], Rodrigo Pinheiro Araldi[4], Eduardo Pagani[3], Irina Kerkis[2]*

[1]*Laboratory of Genetics, Butantan Institute, São Paulo, SP, Brazil.*

[2]*Genetics Laboratory, Instituto Butantan, São Paulo, SP Zip code 05503-900, Brazil.*

[3]*Azidus Brasil, Valinhos 13271-130, SP, Brazil.*

[4]*Genetics Laboratory, Instituto Butantan, São Paulo 05508-010, Brazil.*

Abstract

Background: The safety and efficacy of therapies based on mesenchymal stroma/stem cells (MSCs) have been well-documented in clinical contexts. However, non-clinical studies assessing biodistribution are essential to ensure the safety and effectiveness of these treatments. This study investigated the biodistribution of human immature dental pulp stem cells (hIDPSCs), which hold promise as a potential treatment for Huntington's disease (HD).

Methods: Transfected with luciferase or labeled with magnetic nanoparticles hIDPSCs were intravenously transplanted hIDPSCs into C57BL/6 mice. Subsequently, bioluminescence imaging (BLI) and inductively coupled plasma mass spectrometry (ICP-MS) were used to quantify in vivo and ex vivo biodistribution at various time points (4h, 24h, 3, 7, and 30 days).

Results: BLI and ICP-MS results revealed the presence of hIDPSCs in the chest, lungs, and head at 4h, 24h, and 3 days post-transplantation. Significantly reduced cell numbers were observed from the seventh day onwards, ultimately becoming undetectable by the 30th day. Remarkably, hIDPSCs not only engrafted into the brain but also persisted in this organ for up to 30 days post-transplantation. These findings underscore the capacity of hIDPSCs to successfully engraft and endure in the brain, suggesting their potential for migration and homing to neural tissues.

Introduction

Cell-based therapies have ushered in numerous opportunities for treating (neuro) degenerative disorders [1–5]. In this realm, mesenchymal stromal/stem cells (MSCs) stand out as the primary protagonists of this innovative therapeutic paradigm.

MSCs, multipotent cells from various adult, perinatal, and fetal tissues [6], exhibit diverse therapeutic properties owing to their shared transcriptomic signature and tissue origins [2,7]. Dental pulp stem cells (DPSCs) represent a unique subset of MSCs that can be sourced from the dental pulp (DP) of deciduous, adult, and wisdom teeth. Stem cells extracted from milk or baby teeth naturally shed, providing an advantageous reservoir of youthful stem cells. However, obtaining substantial quantities of DPSCs from a single donor remains challenging, limiting their widespread systemic application in patients.

With over two decades of expertise, our research group has honed a specialization in isolating and expanding DPSCs derived from deciduous teeth

DOI: 10.55920/JCRMHS.2024.08.001356

[8,9]. Over this substantial timeframe, we have conducted meticulous investigations into their in vitro growth, differentiation capacities, and therapeutic implications. Comprehensive preclinical studies employing animal models that faithfully replicate human diseases or injuries substantiate our findings [10].

We have successfully mastered the isolation of DPSCs using a specialized DP explant method, facilitating cell proliferation through continuous mechanical transfer of DP, thereby yielding human immature dental pulp stromal/stem cells (hIDPSCs) [8,11]. Our findings support the potential of this unique subset of adult MSCs, isolated from the deciduous teeth of children aged between six and twelve years, as promising candidates for treating neurodegenerative disorders [2,8,10,12–15]. This promise stems from their ectomesenchymal origin (neural crest), which inherently triggers hIDPSCs to produce and release various neural factors, including nestin (a marker of neural stem/progenitor cells) [16,17] and high level of brain-derived neurotrophic factor (BDNF, which is depleted in patients with Huntington's disease – HD) [3,11,18]. Despite the observed differences between MSCs derived from various tissues and hIDPSCs, they unequivocally meet all criteria outlined by the International Society for Cellular Therapy for defining multipotent MSCs [19,20].

The hIDPSCs at the fifth passage (P5) constitute the active ingredient of the NestaCell® product, produced Good Manufacturing Practices (GMP), which has previously demonstrated safety and efficacy in preclinical studies for the treatment of neurodegenerative disorders such as Huntington's disease (HD) [3,12,18,21] and Parkinson's disease (PD) [13].

While the safety and efficacy of MSCs, including hIDPSCs, have been established in numerous studies, including meta-analyses of preclinical and clinical trials for various diseases [12–14,18], non-clinical biodistribution studies of cell therapy products are indispensable. These studies are crucial for elucidating the distribution of MSCs and form an integral part of the regulatory requirements for registering of advanced therapy products [22].

For this study, we examined the biodistribution of hIDPSCs, the active ingredient of the NestaCell® product, administered at a dose of 1 X 106 cells per mouse, utilizing the C57Bl mouse strain. Additionally, Huntington's disease (HD) was induced in the mouse model by administering 3-nitropropionic acid (3-NP). We evaluated biodistribution at various time points: 4, 7, and 24 hours (short-term), as well as 3, 7, and 30 days (long-term) post-intravenous administration of the product. Our findings provided compelling evidence that the active component of the NestaCell® product effectively crosses the blood-brain barrier, localizing within the brain, and does not induce any adverse effects. These results support the safety profile of the NestaCell® product, as previously reported in a Phase I clinical trial for Huntington's disease [12].

Materials and Methods

Ethical aspects

The procedures described in the study titled "Biodistribution study of cellular therapy for the treatment of cerebral neurodegeneration" were approved by the Ethics Committee in the Use of Animal of Israeli Hospital Albert Einstein (process number 3475/18) on 8th October 2008. The deciduous teeth used to isolate the hIDPSCs were obtained from children aged 6-12 years under the informed consent of their legal representatives. All procedures involving the deciduous teeth collection were approved by the National Research Ethics Commission (CEP/CONEP, process number 4044844, approved on 7th January 2020, study titled "Clinical extension study for safety and efficacy evaluation of Cellavita-HD administration in Huntington's patient").

Isolation, Cultivation, and Characterization of hIDPSCs (NestaCell® Product)

Human immature dental pulp stromal/stem cells (hIDPSCs) utilized in this investigation were extracted from deciduous teeth of healthy children aged 6 to 12 years old, following the completion of Informed Consent Forms, in accordance with the methodology described by Kerkis et al. [8]. The experimental protocols were sanctioned by the National Research Ethics Commission (CEP/CONEP, process number 4044844). Subsequently, hIDPSCs were cultivated up to the fifth passage, corresponding to the active constituent of the NestaCell® product, in a basal medium (comprising Dulbecco's modified Eagle's medium (DMEM)/Ham's F12, supplemented with 15% fetal bovine serum (FBS-HYCLONE (GE Healthcare Life Science, Illinois, USA), 100 U/mL penicillin, 100 µg/mL streptomycin, 2 mM l-glutamine, and 2 nM nonessential amino acids, all from Gibco, Carlsbad, USA). Verification of the MSC phenotype was conducted in adherence to the criteria outlined by the International Society for Cell Therapy (ISCT) [17]. The hIDPSCs utilized herein exhibited positivity for CD105, CD73, and CD90 markers while negative for CD45, CD34, CD11b, and HLA-DR markers, consistent with our prior studies [3,8,9,15]. The cell manufacturing process adhered to the good manufacturing practices (GMP) mandated by the Brazilian Health Regulatory Agency (ANVISA, RDC 508/21) for advanced therapy products. Cryopreservation of cells was carried out using a cryopreserving medium consisting of 70% DMEM (Gibco, Carlsbad, USA), 20% FBS-HYCLONE (GE Healthcare Life Science, Illinois, USA), and 10% DMSO (Sigma-Aldrich, Saint Louis, USA). The

manufacturing process of NestaCell® is safeguarded under US patent number US20160184366A1. Upon administration of hIDPSCs, the cells were thawed and centrifuged at 200 x g (RCF) at room temperature, with the supernatant discarded. Subsequently, the cells were resuspended in sterile saline (0.9% NaCl solution), constituting the NestaCell® product.

RediFect-FLuc-Puromycin gene transfection and selection of Luc-hIDPSC

To analyze the biodistribution of the active component within the NestaCell® product (hIDPSCs), 50,000 hIDPSCs (in passage 2) were initially seeded per well in 12-well plates (TPP Techno Plastic Products AG, Trasadingen, Switzerland), each containing 200 µL of basal culture medium as previously described. After 12 hours, the culture medium was replaced with an Opti-MEM medium (Gibco, Waltham, Massachusetts, USA), devoid of serum or antibiotics, to facilitate viral transfection. The viral transfection process was initiated according to the protocol provided for RediFect-FLuc-Puromycin Lentiviral Particles (Perkin Elmer, Waltham, Massachusetts, USA, product number CLS960002). These lentiviral particles carry a red-shifted Luciola italica luciferase transgene controlled by the stable UbC promoter, rendering them self-inactivated and recombination incompetent.

For transfection at multiplicities of infection (MOI) of 10 or 20, 10 µL or 20 µL of the viral particle solution (RediFect-FLuc-Puromycin Lentiviral Particles) was added, respectively, to a concentration of 5 × 104 cells. After 24 hours, the medium was aspirated, and the cells were washed twice with phosphate-buffered saline (PBS) (Gibco, Waltham, Massachusetts, USA). Fresh basal culture medium supplemented with 0.5 µg of Puromycin (Thermo Fisher Scientific, Waltham, Massachusetts, USA) was added to select transfected hIDPSCs (puromycin-resistant). The medium containing puromycin was replenished every 3 days for 10 days to ensure effective cell selection.

Following the 10-day selection period, the cells were washed with PBS and expanded in 25 cm^2 culture flasks (Corning, New York, USA) to further propagate the selected hIDPSCs. Simultaneously, an aliquot was plated in duplicate on a 96-well plate (TPP Techno Plastic Products AG, Trasadingen, Switzerland) at various cell concentrations ranging from 5,000 to 50,000 cells per well for 24 hours to confirm successful cell transfection. Luciferin (XenoLight D-Luciferin Potassium Salt, Perkin Elmer, Waltham, Massachusetts, USA) was added. Bioluminescence imaging (BLI) was performed using the IVIS Spectrum In Vivo Imaging System (Perkin Elmer, Waltham, Massachusetts, USA) to visualize the BLI signal and confirm transfection efficacy (Figure A1, Tables A1 and A2).

Upon confirmation of successful cell transfection, the transfected hIDPSCs were transferred to 25 cm2 culture flasks (Corning, New York, USA) for expansion to the fifth passage (P5), which corresponds to the active component of the NestaCell® product.

Obtaining of magnetic nanoparticle (MNP)-hIPDSCs

Moreover, hIDPSCs were labeled with magnetic nanoparticles (MNPs). To achieve this, 1 × 105 cells were seeded per well in a 24-well plate, with each well containing 2 mL of basal culture medium. After 24 hours, 40 µg/mL of MNPs were added to the culture. Following an 18-hour incubation period, the hIDPSCs underwent two washes with 500 µL of PBS and were then fixed with 500 µL of 4% paraformaldehyde (4% PFA) (Sigma-Aldrich, Sant Louis, USA) for two hours. Subsequently, the cells were stained with 1 mL of Prussian blue for five minutes to assess the efficiency of MNP internalization by hIDPSCs. Prussian blue staining solution was prepared by reacting 5% HCl with KFe[Fe(CN)6], resulting in the final solution K4Fe[Fe(CN)6HCl] (which was added to the wells). The MNP core reacted with K4Fe[Fe(CN)6HCl], forming a blue-green precipitate. The cells were then dehydrated with 70%, 95%, and 100% alcohol for 30 seconds each. Subsequent images of the MNP-labeled hIDPSCs were captured using the Eclipse TI-Nikon microscope (Figure A2). The viability of MNP-labeled hIDPSCs was evaluated through MTT and BLI assays (Figure A3).

Animal model

A cohort of 100 C57BL/6 mice was utilized in the present investigation. These mice were procured from the Institute of Biomedical Sciences at the University of São Paulo (USP, São Paulo-SP, Brazil). They were housed within the vivarium of the Surgery Training Center (CETEC) at Israeli Hospital Albert Einstein (São Paulo-SP, Brazil). They were accommodated in polypropylene microisolators (32 × 20 × 21 cm), with five animals per microisolator, within ventilated racks (Alesko®) maintained at 45 air changes per hour. The animal facility was rigorously controlled, maintaining a constant temperature of 23 ± 2ºC, humidity at 48%, and adhering to a 12:12 hour light-dark cycle. Food and water were provided as ad libitum throughout the study. Before to experimentation, the mice underwent a seven-day acclimatization period within the animal facility. All experimental procedures involving animals were conducted during the light phase, between 9:00 and 16:00 h.

Animal Models for Huntington's Disease (HD): The HD animal model was established through intraperitoneal injection of 3-nitropropionic acid (3-NP) [3], a toxin produced by various fungal and plant species. 3-NP is an irreversible inhibitor of mitochondrial succinate dehydrogenase (SDH) [22]. We selected this chemically induced animal model over transgenic mice due to the distinct manifestation of striatal neuron death observed in the 3-NP model compared

to the transgenic model expressing mutated huntingtin. For approximately two decades, it has been recognized that 3-NP induces cell death linked with mitochondrial dysfunction and neurodegeneration, closely resembling the pathological features of HD [22–24]. Furthermore, animals treated with 3-NP display clinical manifestations reminiscent of HD symptoms observed in patients, including dystonia, ataxia, chorea, dementia, bradykinesia, muscle weakness, and rigidity [3,23–25].

In our preclinical investigations for HD, we previously employed the 3-NP model, underscoring its utility in elucidating the distribution of MSCs. Specifically, mice received intraperitoneal treatment with a single dose of 20 mg/kg/day of 3-NP (Sigma-Aldrich, St. Louis, MO, USA) for four consecutive days, as Colle et al. [26] detailed. The 3-NP was diluted in saline and adjusted to a pH of 7.4 with NaOH under aseptic conditions, then stored at 2-8°C away from light.

Mice were divided into six groups (G1 to G6), as delineated in Table 1. Groups 1 and 2 (G1 and G2) were exclusively administered saline (the vehicle for the NestaCell® product). Groups 3 and 5 (G3 and G5) received intravenous treatment with a single dose of NestaCell® product at a concentration of 1 X 105 hIDPSCs/animal; however, these groups were omitted from the study as this cell concentration failed to produce detectable bioluminescent signals. Groups 4 and 6 (G4 and G6) received intravenous treatment with a single dose of 1 X 106 hIDPSCs/animal. Notably, G4 comprised 3-NP-treated mice (HD animal model), while G6 comprised healthy mice.

In vivo transplantation of Luc-hIDPSC or MNP-hIDPSC

The hIDPSC transfected with luciferase (Luc-hIDPSC) or labeled with MNP (MNP-hIDPSC) were intravenously administrated in the animal groups 4 and 6 (Table 1). As control, we used sterile saline (groups 1 and 2, Table 1), which is used as administration vehicle of the NestaCell® product. For the administration of Luc-hIDPSCs, MNP-hIDPSCs or placebo, the animals were anesthetized with 100mg/kg of ketamine (Cetamin®, Syntec, Brazil) and 10mg/kg of xylazine (Xilazin®, Syntec, Brazil), and maintained with inhalational anesthesia of isoflurane (Cristália DCB 1565.01, Brazil) at a concentration of 2%. To ensure that the animals remained anesthetized, respiratory rate, immobility and loss of reflexes were evaluated. Then, Luc-hIDPSC, MNP-hIDPSC or saline solution were administered intravenously into the retro-orbital sinus using a 27G scalp and Pump Elite11 infusion pump with an approximate volume of 150 µL for 3 minutes, with flow of 50 µL/minute. To ensure greater comfort, the animals were kept warm with a thermal blanket until the end of the procedure and return of the anesthetic.

Assessment of biodistribution using the bioluminescence image technique

For bioluminescence imaging (BLI) acquisition, animals were anesthetized with 5% isoflurane and maintained under 2% isoflurane using the XGI-8 system (Perkin Elmer, Waltham, Massachusetts, USA). Subsequently, 450 mg/kg of D-Luciferin was intraperitoneally injected 10 minutes before initiating image acquisition on the IVIS Lumina II system (Perkin Elmer, Waltham, Massachusetts, USA). Each animal was positioned within the imaging chamber, featuring a 12.5 cm field of view, a binning factor of 2, an F1 camera lens aperture size to optimize sensitivity, and a photographic exposure time of 1 second. A series of BLI images were captured over 10 minutes to identify the peak signal, with an integration time of three minutes per image for one hour. Image analysis was conducted in absolute radiation units (photons/seconds) using Living Image 4.5.2 software (Perkin Elmer, Waltham, Massachusetts, USA).

Quantification of iron load using the ICP-MS technique

The inductively coupled plasma mass spectrometry (ICP-MS) technique, utilizing the Perkin Elmer NexiON 350x instrument, was employed to quantify magnetic nanoparticles (MNPs) indirectly by assessing the distribution of hIDPSCs. Evaluation via ICP-MS was specifically

Table 1: *Experimental design*

					Number of animals per time point				
Group	**Model**	**Treatment**	**Volume/Dose**	**N[3]**	**4h**	**2h**	**3 days**	**7 days**	**30 days**
G1[1]	3-NP	Saline	150 µL	10	10	10	10	10	10
G2[1]	Heath	Saline	150 µL	10	10	10	10	10	10
G3*	3-NP	NestaCell®	1 X 10^5 cells/animal	10	10	10	10	10	10
G4[2#]	3-NP	NestaCell®	1 X 10^6 cells/animal	50	10	10	10	10	10
G5*	Health	NestaCell®	1 X 10^5 cells/animal	10	10	10	10	10	10
G6[2]	Health	NestaCell®	1 X 10^6 cells/animal	10	10	10	10	10	10

[1]Groups 1 and 2 (G1 and G2) were only treated with the saline (placebo)
[2]Groups 4 and 6 (G4 and G6) were treated with the hIDPSCs. These groups were dedicated to the biodistribution analysis. Each group received a single dose of 1 X 10^6 hIDPSCs/animal
[3]Total number of animals used per group (N)
**These groups were removed from the study because the cell concentration used produced no detectable bioluminescent signal.*
#Only group 4 (G4) were analyzed by the ICP-MS technique and histology

conducted within the G4 group, where 3-NP induction and administration of MNP-hIDPSC occurred. Following retro-orbital sinus administration (equivalent to intravenous delivery), the presence of MNP-hIDPSCs reaching the brain was quantified upon euthanasia on days 3, 7, and 30 post-administrations. Brain tissues were extracted and subjected to processing in a Titan microwave system for subsequent MNP quantification, employing a calibration curve for accuracy (Figure A4).

Digestion of brain and other organ's samples

Digestion of brain, liver, and spleen tissues using a microwave oven involves a rapid and efficient method to break down biological samples. Each piece weighed approximately 0.5 g, and the brains and tissues from other studied organs were isolated and submerged in 10 mL of 70% nitric acid within Teflon vessels. These vessels were then sealed and subjected to heating in a microwave oven (Titan MPS, PerkinElmer, Waltham, Massachusetts, USA) following a prescribed protocol: 10 minutes to achieve 170°C and 30 bar pressure, followed by 5 minutes at 170°C and 30 bar with 80% microwave power; subsequently, 1 minute to reach 200°C and 30 bar, maintaining 90% microwave power for 20 minutes at 200°C and 30 bar; finally, 1 minute to decrease to 50°C and 30 bar, remaining at 50°C and 30 bar with 0% microwave power for 10 minutes. Following digestion, the vessels were allowed to cool, and the contents were then transferred to volumetric flasks for further analysis [27,28].

Iron load measurement process using the ICP-MS technique

The transferred samples underwent dilution with 20 mL of MilliQ water, achieving a 15X dilution factor to align with the detection range of the instrumentation. Aliquots of the digested brain samples were injected in triplicate into the ICP-MS apparatus for iron content determination. Quantification relied on a calibration curve established using a certified iron standard (1000 µg/mL, 2% HNO3) diluted with MilliQ water. The calibration curve was constructed utilizing five iron standards at concentrations of 0, 5, 10, 20, 30, and 50 ng/mL (ppb) (Figure A4). Iron concentration in the samples was expressed in ppb units by comparing the ratios of iron analyte signal intensities observed in the samples to those of the calibration standards.

Histopathological analysis

The animals were euthanized with a combination of 300 mg/kg ketamine (Cetamin®, Syntec) and 30 mg/kg xylazine (Xilazin®, Syntec) at predetermined time points as per the experimental design. Euthanasia was followed by perfusion to preserve brain tissue integrity. A thoracotomy was performed to expose the heart, and a cannula was inserted into the left ventricle. Hemostatic forceps were used to occlude the abdominal aorta, followed by injecting 0.1 mL of Heparin (Liquemine®) to prevent clotting. Transcardial perfusion with approximately 100 to 150 mL of 0.1M PBS solution at pH 7.2, containing 0.9% NaCl, was conducted for 5 minutes to remove the blood and maintain tissue integrity. Subsequently, perfusion continued for 25 minutes with 300 mL of 4% PFA diluted in 0.2M PBS. Tissue fixation was confirmed by assessing neck and limb stiffness.

The distribution of internalized magnetic nanoparticles (MNP) within hIDPSCs was investigated through histological analyses. The presence of iron was visualized using Prussian Blue staining, counterstained with Nuclear Fast Red. Slide preparation involved immersing the slides with tissue sections sequentially in 85% and 70% alcohol for 5 minutes each, followed by a 1-minute immersion in distilled water. Subsequently, slides were incubated in Prussian Blue solution, covering each section for 40 minutes. After incubation, slides were washed in running water for 2 minutes and immersed in Fast Red solution for 5 minutes. Following another 2-minute wash in running water, slides underwent a dehydration process, successively immersed in 70%, 95%, and 100% alcohol for 30 seconds each, followed by a 1-minute immersion in xylene I and subsequent storage in xylene II until covered with Deckglaser coverslips (24x60mm, Knitell, Germany) and sealed with Entellan. Image acquisition was performed using a Nikon TI optical microscope.

The group of animals that received MNP-hIDPSCs (G4) underwent histological evaluation. Prussian Blue staining was performed on brain, liver, heart, kidney, and intestine sections at 3, 7, and 30-day evaluation periods to visualize the presence of internalized MNPs within hIDPSCs.

Immunohistochemistry

Paraffin-embedded tissue immunohistochemistry (IHC-P) analyses were conducted on mouse brain samples. Following euthanasia, the brains were extracted and fixed in a 10% buffered formalin solution. Subsequently, the fixed material was embedded in paraffin and sectioned. The sections underwent deparaffinization and antigenic retrieval in 0.01 M citrate buffer at 95°C for 35 minutes. Endogenous peroxidase activity was quenched using a 6% hydrogen peroxide solution with two 10-minute baths. Sections were then rinsed three times in buffered saline solution (PBS) (0.137 M NaCl, 0.05 M NaH2PO4, pH 7.4) for 5 minutes each and permeabilized with 0.01% Triton X-100 for 20 minutes. Following permeabilization, sections were washed for 5 minutes in PBS and blocked with a 5% BSA solution (in PBS) for 30 minutes.

Next, sections were incubated overnight at 4°C in a humid chamber with the primary rabbit monoclonal anti-mitochondria antibody (AbCam, Cambridge, UK, reference code Ab.133789). After overnight incubation, slides were

Table 2: *BLI signal observed in groups G4 (with 3-NPA induction) and G6 (without 3-NPA induction) at 4h, 24h, 3, 7 and 30 days after Luc-h IDPSC administration. Data expressed in millions of photons/sec as mean ± standard deviation. N= number of animals evaluated.*

Groups	N	4 hours	24 hours	3 days	7 days	30 days
G4 - (3-NPA) - Chest	10	0.46 ± 0.41	0.44 ± 0.42	0.29 ± 0.25	0	0
G4 - (3-NPA) - Head	10	0.13 ± 0.09	0.19 ± 0.17	0.14 ± 0.08	0	0
G6 - Chest	6	1.04 ± 1.01	0.88 ± 0.82	0.64 ± 0.60	0	0
G6 - Head	6	0.06 ± 0.05	0.07 ± 0.06	0.13 ± 0.12	0	0

washed with PBS and incubated at room temperature in a humid chamber for 1 hour with the secondary antibody, as per the HiDef Detection™ HRP Polymer System Kit No 954D-30 protocol (Cell Marque, Rocklin, CA, USA). After incubation, sections were washed thrice in PBS for 5 minutes each and treated with diaminobenzidine (DAB) for 5 minutes. The material was then washed in distilled water for 5 minutes and counterstained with Harris hematoxylin for 2 minutes. Subsequently, slides were washed with distilled water and immersed in a 0.037 M ammonium hydroxide solution to remove excess hematoxylin. Finally, slides were dehydrated, cleared, and mounted with Paramount Mounting Medium (Dako, Santa Clara, CA, USA).

Brain tissues from at least three animals from each experimental group (G1, G2, G4, and G6) were analyzed. Three sections were obtained and analyzed from each brain. All anti-mitochondria antibody (hAMA)-positive cells in mouse brains were captured. Slides were examined using an Axiophot binocular light microscope (Carl Zeiss, Jena, Germany) with objectives ranging from 10X to 100X. Images were captured using AxioVision software version 4.7.2 (Carl Zeiss, Jena, Germany).

Statistical Analysis

The data were depicted as mean ± standard deviation in the tables, and statistical analysis ensued after confirming the variance homogeneity via Levene's test. Temporal comparisons were conducted through one-way ANOVA and the Bonferroni post-hoc test. All analyses were carried out utilizing parametric tests, preceded by an assessment of normality via the Shapiro-Wilk test. A significance level of 0.05 was applied. Statistical analyses were executed using JASP software v0.14.1 (http://www.jasp-stats.org, accessed in November 2021).

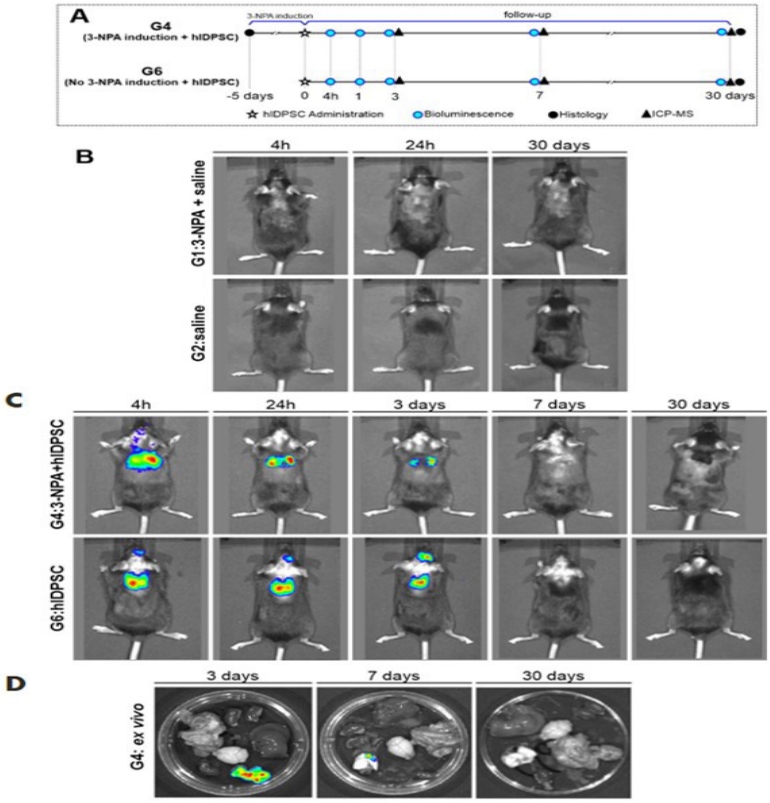

Figure 1: *(A) Experimental design used in the study of biodistribution. G4 (with induction of 3-NPA and administration of hIDPSC) and G6 (without induction of 3-NPA and administration of hIDPSC). Representative image of Luc-hIDPSC biodistribution observed in vivo using BLI assay in groups G1, G2 (B), G4 and G6 at 4h, 24h, 3 days, 7 days and 30 days (C). Representative image of Luc-hIDPSC biodistribution observed ex vivo using BLI assay in group G4 (D).*

Table 3: *Quantification by ICP-MS of MNP-hIDPSC in the organs of animals in the G4 group at 3, 7 and 30 days after its administration. Data expressed in 10,000 cells as mean ± standard deviation. As 10,000 cells correspond to 1% of the total of 1 million administered cells, the numbers also represent a percentage of the administered total. N=number of animals that provided organs for quantification.*

Organ	3 days N=6	7 days N=4	30 days N=3
Lung	44.50 ± 3.95	13.38 ± 0.16	0.35 ± 0.18
Liver	4.34 ± 1.94	3.15 ± 0.50	0.21 ± 0.18
Kidney	2.72 ± 0.79	1.56 ± 0,45	0.10 ± 0.05
Brain	2.02 ± 0.92	1.44 ± 0.51	0.65 ± 0.19
Heart	1.15 ± 0.57	0.57 ± 0.19	0.06 ± 0.02

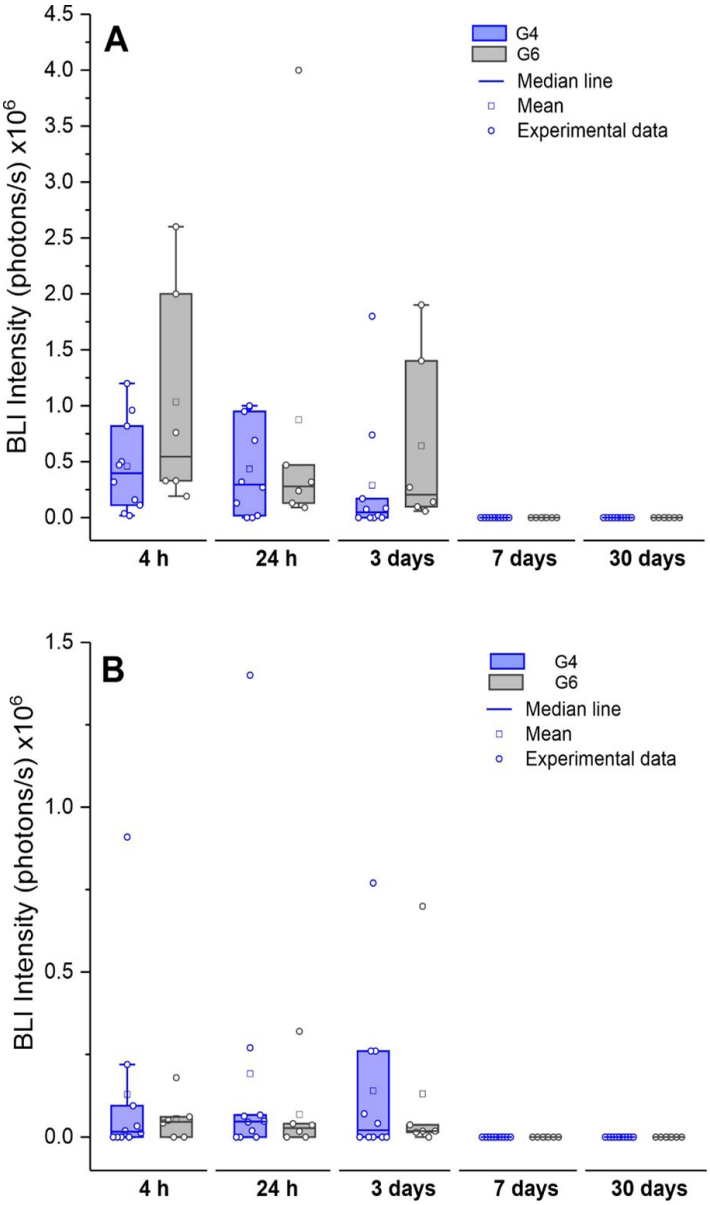

Figure 2: *Distribution (box plot) of Luc-hIDPSC BLI signal intensities in the head in groups G4 (with 3-NPA induction) and G6 (without 3-NPA induction) at short times 4 h, 24 h, 3 days, and long 7 days, and 30 days in chest (A) and brain (B).*

Table 4: *Comparison of samples between times 3, 7 and 30 days by Post Hoc test after one-way ANOVA test, for each organ. Data expressed in 10,000 cells as mean ± standard error. As 10,000 cells correspond to 1% of the total of 1 million administered cells, the numbers also represent a percentage of the administered total. N= number of animals that provided organs for quantification.*

Organ	Comparison between times (days)		Mean Difference	Standard Error	t	*p*
Brain	3	7	0.57	0.48	1.19	0.49
	3	30	1.37	0.53	2.59	0.06
	7	30	0.80	0.57	1.39	0.38
Liver	3	7	1.19	0.90	1.32	0.42
	3	30	4.13	0.99	4.18	0.01
	7	30	2.94	1.07	2.75	0.05
Kidney	3	7	1.16	0.40	2.95	0.04
	3	30	2.62	0.43	6.07	< .001
	7	30	1.46	0.47	3.12	0.03
Heart	3	7	0.59	0.27	2.17	0.13
	3	30	1.10	0.30	3.72	0.01
	7	30	0.51	0.32	1.61	0,29
Lung	3	7	31.12	1.80	17.27	< .001
	3	30	44.15	1.98	22.36	< .001
	7	30	13.03	2.13	6.11	< .001

Results

Biodistribution of hIDPSC by BLI in G1, G2, G4 and G6

After confirming the efficacy of hIDPSC transfection with luciferase (Luc-hIDPSCs) in vitro and determining the maximum intensity of bioluminescence for each cell concentration (Figure A1, Tables A1 and A2), Luc-hIDPSCs were intravenously transplanted into both healthy (G6) and 3-NP-treated mice (G4), which exhibit neuronal degeneration (confirmed by histological analysis, Figure A5). As controls, saline was intravenously administered to healthy (G2) and 3-NP-treated mice (G1). Mice underwent BLI at different time points (Figure 1A). As anticipated, no bioluminescent signal was detected in the animal groups treated with saline (Figure 1B). In contrast, a bioluminescent signal was observed in the head and thorax at 4 hours, 24 hours, and 3 days after cell transplantation (Figure 1C, Table 2). This signal was stronger in the thorax than in the head (Figure 1B, Table 2). Interestingly, the signal was more pronounced in the group induced with 3-NP, exhibiting a

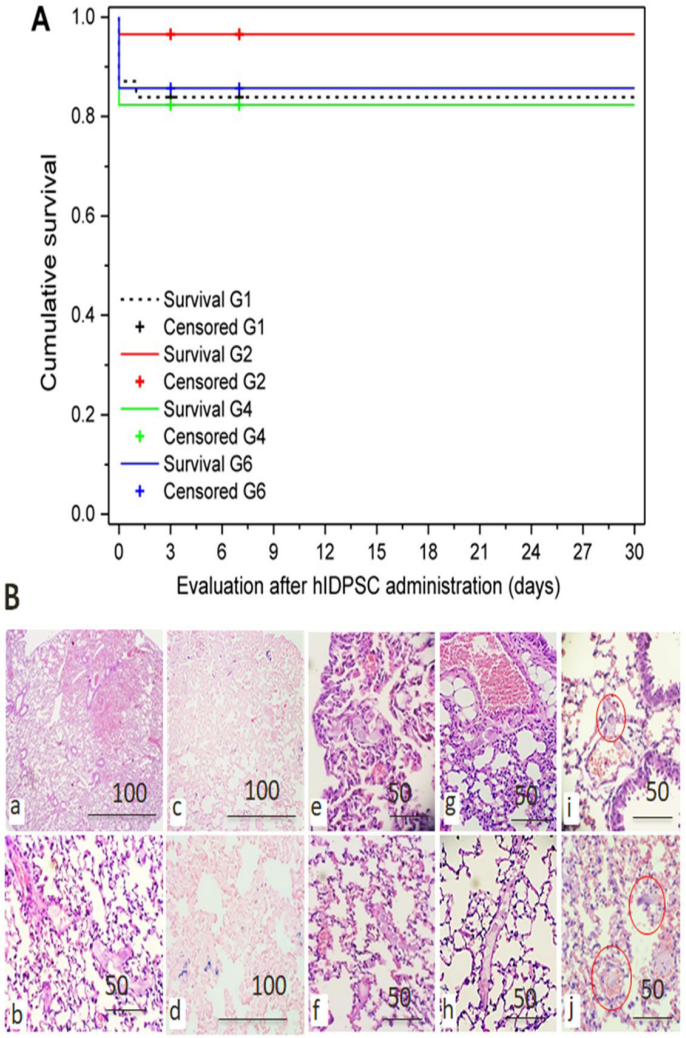

Figure 3: *(A) Survival curves after administration of hIDPSC in G4 and G6 or saline in G1 and G2. The symbol (+) indicates the data measured in each group at times 3, 7 and 30 days. (B) Lung of animal 726_20: Embolization of neuronal, multifocal, mild to moderate neuronal polygonal cytomegalic cells. (A) pulmonary hemorrhage, with embolization of cytomegalic cells (4X); (B) pulmonary hemorrhage, with embolization of cytomegalic cells (10X); (C and D) rare pleomorphic cells (cytomegalic to fusiform amorphous) with little blue granular pigment on Perl's staining, dispersed in the alveolar and perivascular walls, vascular walls and lumen (4X); (E and F) embolization of cytomegalic cells (20X); (G) polygonal cytomegalic cells in the alveolar wall, pulmonary arteries and arterioles (10X); (H) polygonal cytomegalic cells in the alveolar wall, pulmonary arteries and arterioles (40X); (J and K) Pleomorphic cytomegalic intravascular cells with ample cytoplasm, occasional cytomegalic and large conspicuous nucleoli (40X). Staining with HE.*

bioluminescent ratio (thorax/head) of 17-fold compared to the non-induced 3-NP group, which showed a ratio of 3.5-fold. However, the bioluminescent signal ratio (thorax/head) significantly decreased 24 hours after cell transplantation (Figures 1C and 2). In the ex-vivo evaluation, the BLI signal was detected in G4 until the 7th day, only in the lungs, with a mean intensity of 0.04 million photons/s (Figure 1D).

Biodistribution of hIDPSC demonstrated by ICP-MS in G4 and G6

Following the intravenous injection of MNP-hIDPSCs in G4 animals treated with 3-NPA, we observed that after 3 days, approximately 45% of these cells were localized in the lungs, with the remaining cells distributed in smaller proportions among various organs. A gradual decrease in cell numbers was noted over time (from 3 to 30 days) across all evaluated organs (Figure 2). The ANOVA test revealed a significant decrease in cell numbers over time for the liver ($p=0.006$), kidney ($p<0.001$), heart ($p=0.011$), and lung ($p<0.001$). In contrast, the variation in brain cell numbers was not significant ($p=0.075$) (Table 3, Figure 3A). These findings suggest a slower decline of MNP-hIDPSCs in the brain than other organs.

Table 4 illustrates the differences in cell quantities observed in each organ at 3 vs. 7 days, 3 vs. 30 days, and 7 vs. 30 days post-administration of hIDPSCs in the brain, liver, kidney, heart, and lung. Significance was observed threefold in the lungs ($p<0.001$) across all evaluated time points and in the kidney at 3 vs. 30 days ($p<0.001$). However, no significant differences were noted between the time points in the brain, liver, and heart (Table 4).

Following the intravenous administration of MNP-hIDPSCs into G6 animals, a significant presence of cells was observed in the lungs of mice after 4 hours, gradually decreasing over time until reaching minimal levels at 30 days. This trend was mirrored across all organs, with initial cell accumulation noted primarily in the liver, followed by the kidney, heart, and brain (Table A3, Figure A6).

ICP-MS analysis of G6 corroborated the findings of G4, indicating an accumulation of cells in the lung at 4 hours post-administration, with subsequent reductions over time. In other organs, such as the liver, kidney, and heart, cells were detected via the ICP-MS technique, albeit in smaller quantities. Notably, the brain exhibited the lowest cell counts recorded at all time points, further decreased compared to G4.

Survival after administration of hIDPSC or saline in G1, G2, G4 and G6

As depicted in Figure 4A, survival rates, body weight trajectories, and clinical and behavioral outcomes did not exhibit significant differences among the four groups monitored for 30 days.

Two animals, both from G4 (3-NPA induced), succumbed immediately following the administration of the investigational product. One animal exhibited pulmonary embolization characterized by pleomorphic cytomegalic cells with extensive vacuolated cytoplasm. These emboli

Citation: *Cristiane Wenceslau Valverde. Assessing the Biodistribution of Human Immature Dental Pulp Stem Cells (NestaCell®) via Intravenous Administration in Mice: A Non-Clinical Investigation . Jour of Clin Cas Rep, Med Imag and Heal Sci 8(4)-2024.

DOI: 10.55920/JCRMHS.2024.08.001356

were dispersed throughout the pulmonary vasculature and alveoli. The cells, ranging from small to moderate in number, measured 50 to 100 micrometers in diameter, featuring ample, poorly defined cytoplasm, pleomorphic nuclei, and prominent nucleoli. Although displaying dimensions and characteristics typically associated with dysplastic cells, they did not entirely correspond to megakaryocytic cells' staining and nuclear features. Many of these cells exhibited granular pigments of variable sizes, which stained blue with Perl's stain, suggesting an association with MNP-hIDPSCs. Cells with such attributes were not observed in other organs. A few round cells staining positive with Perl's stain, consistent with lung macrophages, were also identified (Figure 4B).

The second animal perished shortly after hIDPSC administration, albeit without pulmonary embolization. Instead, severe neurological damage attributable to 3-NP treatment was evident in this case.

Histopathological evaluation of animals induced with 3-NPA (G4) and treated with hIDPSC

The histopathological investigation focused solely on G4 animals. As anticipated, following 3-NPA administration, a spectrum of histological changes spanning multiple organs was observed, most discreetly heterogeneous and not discernible macroscopically.

No severe neurological lesions were evident except in one animal induced with 3-NPA, which succumbed shortly after product administration. Remarkably, this animal exhibited bilateral symmetrical degenerative lesions in regions between cerebellar nuclei and cerebellar white matter, with no evidence of MNP-hIDPSC positivity in Perl's stain, a technique used to demonstrate ferric salts in tissue (Figure 5A).

As expected, chronic inflammatory lesions were noted in the serosa of various abdominal organs in 3-NPA-induced animals, often without extending into the underlying parenchyma or with minimal subserosal extension. Substantial histological changes were observed in most 3-NPA-induced animals, with nine displaying mild changes of low clinical relevance. Lesions affected organs randomly among subjects, predominantly involving the liver, pancreas, small or large intestine, perirenal, and periurogenital tissue. These lesions were characterized by multiple foci of subacute to chronic inflammatory lesions, predominantly affecting the abdominal serous surface, suggestive of reactive lesions possibly due to local chemical insult. Such lesions were frequently observed in the peri-urogenital region, liver, pancreas, and large intestine (Figure 5B). Notably, these lesions were absent in animals evaluated after 30 days of hIDPSC administration, indicating a potential anti-inflammatory activity of the NestaCell® product.

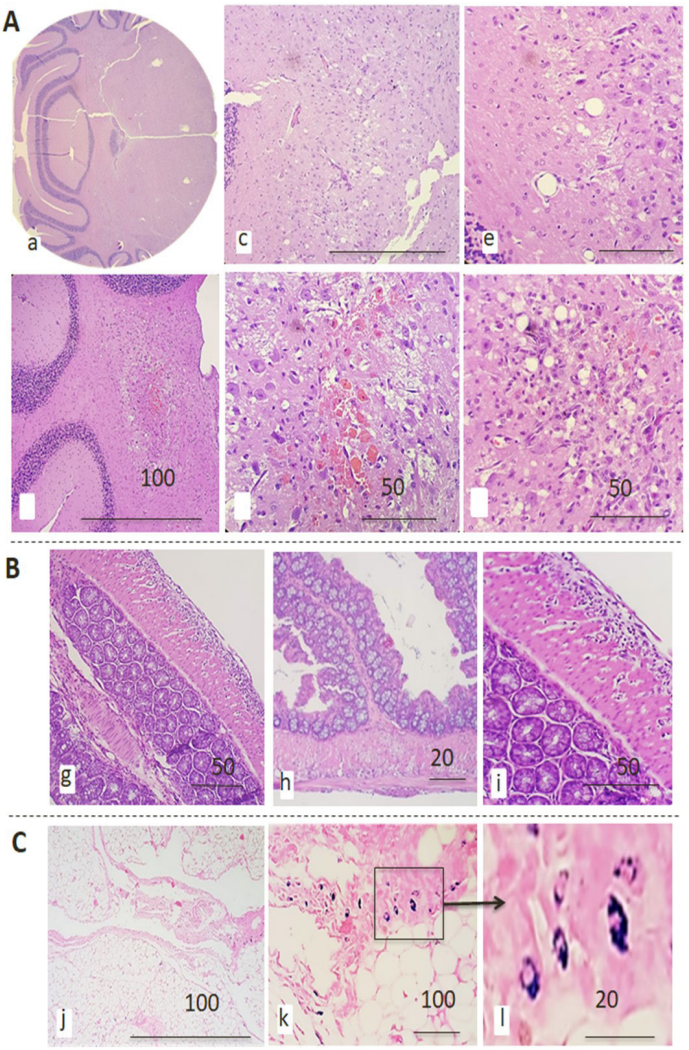

Figure 4: *(A) Cerebellum of animal 730-20 (G4). (A-F) HE staining: focal, bilateral, symmetrical, neuronal and neutrophil vacuolization, with gliosis, neovascularization, hemorrhage, and erythrophagocytosis. (B) Animal 733_20, G4, evaluated 3 days after the CTIPDh administration. (A), (G) mural colitis, lymphocytic (4X); (H) mural leiomyodegeneration, with fibrinous serositis, colon (10X); (J) Mural, lymphocytic colitis (40X). (C) Animal 653_20, G4. Pelvic adipose tissue staining (K): group of perivascular fusiform to stellate cells with abundant Perl's + pigment, (l): high magnification of inset in (K).*

Spindle cells resembling fibroblasts were identified as reactive mesothelium, showing no evidence of ferric granular pigment. However, in one animal evaluated seven days post-hIDPSC transplantation, an influx of fusiform to stellate cells with abundant Perl's-positive pigment was observed without apparent inflammatory or hemorrhagic processes. This finding raises suspicion about the potential presence of hIDPSCs dispersed within peritoneal lesions, suggesting a tropism of hIDPSCs for injured tissues (Figure 5C).

Immunohistochemical study of hIDPSC biodistribution in mice brain

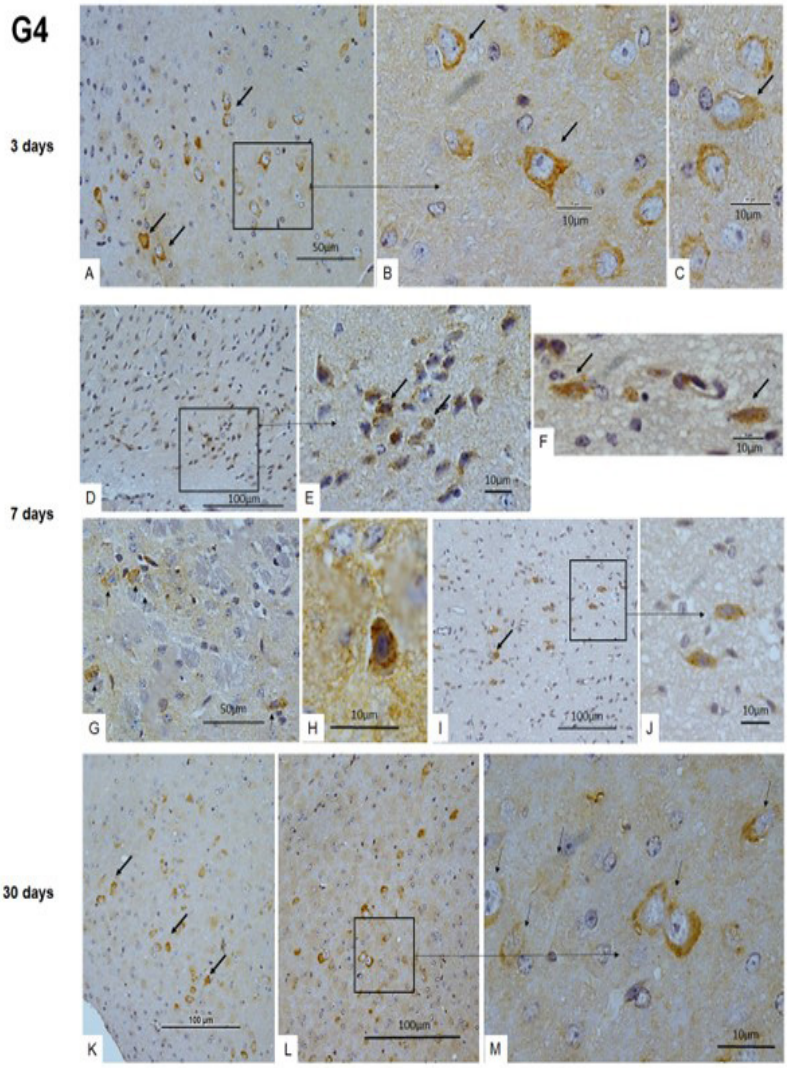

Figure 5: *Representative figure. Immunohistochemistry demonstrated the biodistribution of hIDPSC in the brain of mice (C57Bl), in G4 (3NPA+hIDPSC), 3, 7 and 30 days after hIDPSC intravenous (IV) administration using a specific anti-human mitochondrial antibody (hAMA) (A-M). (A-C) 3 days after hIDPSC IV administration demonstrates hAMA-positive hIDPSC (brown) in the cortex, whereas mouse cells did not show this stain. Animal number 734-4b. (D-J) 7 days after hIDPSC IV administration demonstrates hAMA-positive hIDPSC in the cortex (D-F), in the striatum (G-H) and in thalamus (I, J). Animal number 2813-1. (K-M) 30 days after hIDPSC IV administration demonstrates hAMA-positive hIDPSC (brown) in the cortex. Animal number 670-4b. Note that the hIDPSC have fibroblastic morphology and their size is larger than that of mouse cells; they are always found in groups or at least in pairs. Black arrows indicate hAMA positive hIDPSC. Black quadrat shows selected area presented in high magnification. Scale bar (A, G, I) = 50 µm, (B, C, E, F, H, J and M) = 10µm, (D, K, L) = 100 µm. The nuclei were stained with hematoxylin and eosin (HE).*

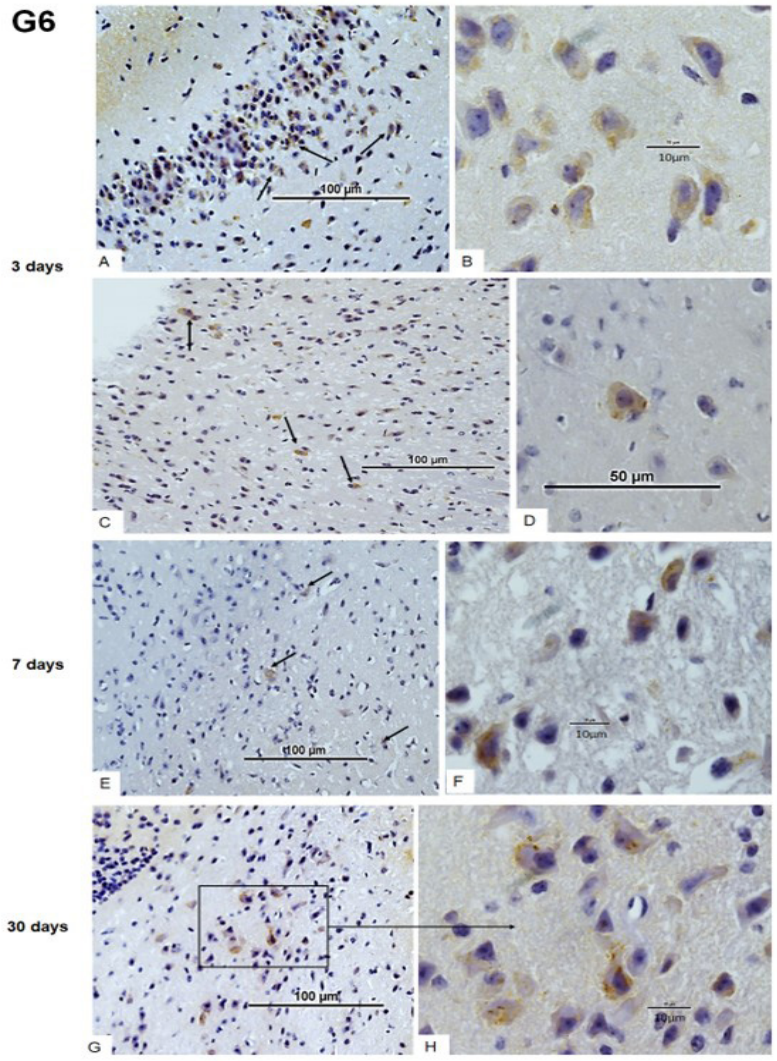

Figure 6: *Representative figure. Immunohistochemistry demonstrated the biodistribution of hIDPSC in the brain of mice (C57Bl), in G6 (+hIDPSC), 3, 7 and 30 days after hIDPSC intravenous (IV) administration using a specific anti-human mitochondrial antibody (hAMA) (A-M). (A-D) 3 days after hIDPSC IV administration demonstrates hAMA-positive hIDPSC (brown) in the cortex (A, B) and thalamus (C, D), whereas mouse cells did not show this stain. Animal number 2391-19b. (E, F) 7 days after hIDPSC IV administration demonstrates hAMA-positive hIDPSC in the cortex. (G, H) 30 days after hIDPSC IV administration demonstrates hAMA-positive hIDPSC in the cortex. Animal number 2401-19b. Note that the hIDPSC have fibroblastic morphology and their size is larger than that of mouse cells; they are always found in groups or at least in pairs. Black arrows indicate hAMA positive hIDPSC. Black quadrat shows selected area presented in high magnification. Scale bar: (A, C, E, G) = 100 µm, (B, F, H) = 10µm, (D) = 50 µm. The nuclei were stained with hematoxylin and eosin (HE).*

Citation: *Cristiane Wenceslau Valverde. Assessing the Biodistribution of Human Immature Dental Pulp Stem Cells (NestaCell®) via Intravenous Administration in Mice: A Non-Clinical Investigation . Jour of Clin Cas Rep, Med Imag and Heal Sci 8(4)-2024.

DOI: 10.55920/JCRMHS.2024.08.001356

To validate the presence of hIDPSCs within the murine brain, we conducted immunodetection targeting a specific cell antigen for human cells, the human anti-mitochondrial antibody (hAMA). Our analyses affirmed the presence of hIDPSCs in the brains of both G4 (3-NPA induced) and G6 groups, which received intravenous administration of hIDPSCs.

In G4, on day 3, hIDPSCs were detected in the cortex (Figures 6A-C); on day 7, they were observed in the cortex (Figures 6D-F), striatum (Figures 6G, H), and thalamus (Figures 6I, J); and on day 30, they persisted in the cortex (Figures 6K-M). Similarly, in G6, on day 3, hIDPSCs were found in the cortex (Figures 7A, B) and thalamus (Figures 7C, D); on days 7 (Figures 7E, F) and 30 (Figures 7G, H), they were localized in the cortex.

Positive staining for hAMA in hIDPSCs appeared intracellularly, evenly distributed within the cytoplasm (Figures 6A-M and 7A-H). These cells were either clustered or found individually, exhibiting a fibroblastic morphology with prominent nuclei. hIDPSCs displayed a consistent cell size ranging from 10µm to 15µm, larger than that of mouse cells, facilitating their discernment among mouse cell populations (Figures 6B, C, H, M, and 7B, D, F, H).

Figure A7 presents appropriate positive and negative controls: hAMA-positive labeling observed in hIDPSCs (Figure A7A) and control for nonspecific binding of the secondary anti-rabbit antibody, demonstrating the absence of staining upon omission of the primary antibody (hAMA) (Figure A7B). Notably, hAMA-positive cells were absent in the brains of control animals from G1 and G2, which did not receive hIDPSC administration (Figure A7C-H).

Discussion

The biodistribution analysis of hIDPSCs was conducted using both bioluminescence imaging (BLI) and inductively coupled plasma mass spectrometry (ICP-MS) techniques at various time points in groups G4 (3-NPA-induced mice) and G6 (healthy mice). Additionally, ICP-MS was exclusively employed in the G4 group at 3-, 7-, and 30-days post-administration.

BLI revealed that immediately following intravenous administration, Luc-hIDPSCs were predominantly localized in the thorax, with lesser accumulation in the head, a phenomenon more pronounced in G6. However, cell numbers declined after 24 hours, particularly in the thorax, whereas they remained relatively stable in the head.

ICP-MS analysis demonstrated that approximately 50% of the administered cells remained in the lungs at day 3 post-administration. By this point, the heart, brain, kidneys, and liver contained just over 1%, 2%, 3%, and 4% of the administered cells. These distribution patterns align with the expected blood flow distribution through the various branches of the aorta. Subsequent analyses revealed a decline in cell numbers across all tissues over time, with the most significant reduction observed in the lungs and the least in the brain. Notably, even after 30 days, the brain retained approximately one-third of the cells observed on day 3, while the lungs harbored less than 1%.

The integrated assessment of biodistribution using BLI and ICP-MS techniques suggests an immediate pulmonary entrapment of administered cells, predominantly in the lungs. These findings are consistent with previous studies investigating the biodistribution of bone marrow or adipose tissue derived MSCs. Upon intravenous administration, a substantial proportion of MSCs (~50–80%) are typically home to the lungs initially, a phenomenon attributed to their relatively large size (~20–30 µm in diameter), which exceeds the diameter of pulmonary capillarie [29].

The decrease in the number of cells trapped in the lung following a vasodilator's administration supports the hypothesis that MSC size plays a pivotal role in the first-pass effect [30,31]. This phenomenon has been extensively investigated to assess the potential therapeutic efficacy of MSCs in various preclinical lung disease models. Studies have consistently shown that irrespective of the severity of lung disease and the delivery route, MSCs do not persist in the respiratory tract beyond 24 hours but still exert therapeutic effects [32–34].e

Following the initial pulmonary entrapment, the cells are distributed among all organs, likely in proportion to each organ's share of the cardiac output. However, our study revealed a progressive increase in cell concentration in the head over the first 3 days, concomitant with a decreased lung concentration. Indeed, ICP-MS analysis indicated that by the 3rd day, approximately 2% of the total administered cells were located in the brain. Moreover, over the subsequent 30 days, the decline in cell numbers within the brain occurred much slower than in other organs, particularly the lungs. Although not statistically significant, this collective data suggests a potential tropism of hIDPSCs towards the central nervous system (CNS).

The biodistribution patterns of MSCs observed in preclinical studies have been corroborated by human investigations. For instance, Koç et al. [35] demonstrated that intravenous administration of MSCs was well tolerated in patients, with a dose of 1x106 MSC/kg body weight. However, MSC tracking in patients with breast carcinoma revealed detection only in the bloodstream. This finding was further substantiated in patients with liver cirrhosis, where 111in-oxin-labeled MSCs, a diagnostic radiopharmaceutical, initially accumulated in the lungs, followed by escalating accumulation in the liver and spleen up to day 10 post-

Citation: *Cristiane Wenceslau Valverde. Assessing the Biodistribution of Human Immature Dental Pulp Stem Cells (NestaCell®) via Intravenous Administration in Mice: A Non-Clinical Investigation . Jour of Clin Cas Rep, Med Imag and Heal Sci 8(4)-2024.
DOI: 10.55920/JCRMHS.2024.08.001356

administration [36]. The proportion of cells accumulating in the lungs decreased from approximately 35% shortly after transplantation to 2% or less by day 10, while the spleen exhibited the highest cell accumulation at this time point. These results underscore a discernible biodistribution pattern of MSCs in the lungs, liver, and spleen in human subjects, akin to findings in animal models.

Another intriguing question pertains to whether hIDPSCs exhibit tropism for injured and/or inflamed tissues. In one animal evaluated 7 days post-hIDPSC administration, positive Perl cells were detected in peritoneal lesions. In the BLI study, within the initial 4 hours following Luc-hIDPSC administration, the ratio of cell concentration in the chest to the head was 17-fold higher in induced animals compared to non-induced animals, indicating a pronounced tropism. Conversely, the head-to-lung ratio was approximately 5-fold higher in 3-NPA-induced animals compared to non-induced animals. Notably, induced animals exhibited CNS lesions, with hIDPSCs in their brains exhibiting higher concentrations than those in non-induced animals.

Intravenously administered bone marrow MSCs have demonstrated the ability to migrate into damaged brain tissue via the middle cerebral artery, as evidenced by their presence 7 days post-transplantation, leading to improved neural function in ischemic rats [37]. Similarly, other studies have corroborated the migration of MSCs to the brain following intravenous infusion [38]. Utilizing intravital microscopy and BLI in a murine experimental autoimmune encephalitis model, the accumulation of transplanted MSCs in brain vessels within inflammatory foci of experimental autoimmune encephalomyelitis was observed 16- and 30-days post-transplantation [39]. While the exact numbers of engrafted MSCs remain undetermined and may be relatively low, these findings suggest that active inflammation can alter the MSC homing pattern in inflamed anatomical sites from nonspecific entrapment to recruitment [40]. Another study investigated the biodistribution of hDPSCs from impacted third molars in 7-week-old male BALB/c nude mice. Administering 1 × 105 hDPSCs intravenously via the tail vein, the cells initially amassed in the lungs but decreased within 24 hours. Sparse hDPSCs were also found in the heart, spleen, kidney, and brain [41].

Although hIDPSCs are similar to MSCs derived from bone marrow, adipose tissue, or the umbilical cord, they also possess unique characteristics. Our investigation revealed that their homing and biodistribution patterns closely resemble other MSCs [6,42].

Furthermore, we assessed macroscopic and microscopic lesions in animals subjected to 3-NPA induction (G4) and treated with hIDPSCs across various organs. Notably, we observed significant pathological changes in most animals induced with 3-NPA. These changes manifested as multiple foci of subacute to chronic inflammatory lesions, predominantly affecting the abdominal serous surface, indicative of reactive lesions likely due to local chemical insult. Spontaneous individual lesions of minor relevance, commonly observed in the species, were also identified.

This study also recorded two fatalities immediately after administration, a matter of considerable toxicological interest, particularly in predicting potential adverse events in human subjects. One animal succumbed to a pulmonary embolism linked to hIDPSC administration. Notably, hIDPSCs have been utilized in clinical trials with approximately 800 intravenous administrations to humans (data pending publication, Regulatory Report), where no adverse events consistent with pulmonary embolism were reported.

We postulate that in the case of this specific animal, cell agglutination into clumps occurred before administration. These clumps subsequently formed thrombi, which led to pulmonary embolism upon migration through the venous circulation. The likelihood of such clump formation is substantially greater in animal models compared to clinical studies, primarily due to the proportionately higher doses administered to mice than to humans. In clinical trials, humans typically receive 1 or 2 million cells per kilogram of body weight. However, the animals in our study, weighing approximately 17-20 grams, were administered a total dose of 1 million cells, equivalent to approximately 60- to 120-fold the human dose. This dosage was selected due to constraints associated with the BLI signal collection technique.

Initially, the study included two groups (G3 and G5) to which a total dose of 100,000 cells was administered. However, no detectable bioluminescent signal was observed in these animals. Consequently, the decision was made to administer a dose of 1 million cells per animal.

This study also documented two fatalities immediately following administration, a subject of significant toxicological interest, especially concerning the prediction of potential adverse events in human subjects. One animal succumbed to a pulmonary embolism associated with hIDPSC administration. Notably, hIDPSCs have been employed in clinical trials with approximately 800 intravenous administrations to humans (data pending publication, Regulatory Report), where no adverse events consistent with pulmonary embolism were reported.

We hypothesize that in the case of this animal, cell agglutination into clumps occurred before administration. Subsequently, these clumps formed thrombi, which resulted in pulmonary embolism upon migration through the venous circulation. The likelihood of such clump

Citation: *Cristiane Wenceslau Valverde. Assessing the Biodistribution of Human Immature Dental Pulp Stem Cells (NestaCell®) via Intravenous Administration in Mice: A Non-Clinical Investigation . Jour of Clin Cas Rep, Med Imag and Heal Sci 8(4)-2024.
DOI: 10.55920/JCRMHS.2024.08.001356

formation is significantly higher in animal models than in clinical studies, primarily due to the proportionately higher doses administered to mice than to humans. In clinical trials, humans typically receive 1 or 2 million cells per kilogram of body weight. However, the animals in our study, weighing approximately 17-20 grams, were administered a total dose of 1 million cells, equivalent to approximately 60- to 120-fold the human dose. This dosage was selected due to constraints associated with the BLI signal collection technique.

Initially, the study included two groups (G3 and G5) to which a total dose of 100,000 cells was administered. However, no detectable bioluminescent signal was observed in these animals. Consequently, the decision was made to administer a dose of 1 million cells per animal.

Conclusions

We have demonstrated that following intravenous administration into both healthy and 3-NPA-induced animals, hIDPSCs exhibit an initial tropism towards the lungs, consistent with previous findings concerning MSCs. Upon traversing the pulmonary circulation, these cells disseminate throughout the systemic circulation, likely in accordance with the distribution of cardiac output to various anatomical sites. Over the period spanning from the 3rd to the 30th-day post-administration, there is a reduction in the number of cells present in all examined tissues. Notably, this decline is less pronounced in the brain compared to other tissues. Only 2% of the administered cells are initially detected in the brain. However, by the 30th day, approximately 33% of this initial fraction remains detectable within brain tissue. In contrast, the proportional decrease in cell numbers is substantially greater in all other examined tissues. These findings suggest a distinctive affinity of hIDPSCs for the brain, implying a potential therapeutic avenue for neurological disorders.

Author Contributions: C.W.V. carried out the study design and drafted the manuscript. LFG was responsible for the project management, cells labeling with magnetic nanoparticles, BLI and IC-PMS studies, and performed the statistical analysis. V.F.G. was responsible for the cell transfection with luciferase and cell culture. A.P.G. was responsible for the histopathological studies. B.O.P. was responsible for the cell culture and maintenance. L.C. coordinated the in vivo studies. C.F. was responsible for the animals handling. L.H.Y. performed the statistical analysis. L.F. was responsible for the study design. R.P.A. was responsible for the study analysis and drafted the manuscript. I.K. was responsible for the experimental study design, analysis, and final approval.

Funding: This study was funded and supported by Grants from the Butantan Foundation, São Paulo-SP, Brazil and Cellavita Pesquisas Científicas Ltd., Valinhos-SP, Brazil by the financial support.

Conflicts of Interest: The authors declare no conflict of interest.

Significance Statement: Although the safety and efficacy of mesenchymal stem cells (MSCs) had already demonstrated in both human and non-human (or in vivo studies with animal models), Regulatory Agencies require that MSCs candidates to rich the market as therapeutic products be extensively studied. As part of this studies is the non-human biodistribution assay. This study analyzed the capacity of human immature dental pulp stem cells (hIDPSCs), a special type of MSC, which has been extensively investigated as treatment for Huntington's disease (HD), to reach the brain after the intravenous administration. Using different techniques commonly used to analyze the biodistribution of MSCs, we provided evidence that hIDPSCs are able to migrate (homing) to the brain, remaining withing brain areas naturally affected by HD for at least 30 days.

References

1. Araldi RP, D'Amelio F, Vigerelli H, de Melo TC, Kerkis I. Stem cell-derived exosomes as therapeutic approach for neurodegenerative Ddsorders: From biology to biotechnology. Cells 2020;9:2663. https://doi.org/10.3390/cells9122663.
2. Kerkis I, Araldi R, Wenceslau C, Mendes T. Advances in cellular and cell-free therapy medicinal products for Huntigton's disease treatment. From Physiopatology to Treat. Huntigton's Dis., InTech; 2022, p. 1–27. https://doi.org/10.5772/55358.
3. Wenceslau CV, de Souza DM, Mambelli-Lisboa NC, Ynoue LH, Araldi RP, da Silva JM, et al. Restoration of BDNF, DARPP32, and D2R expression following intravenous infusion of human immature dental pulp stem cells in Huntington's disease 3-NP rat model. Cells 2022;11:1664. https://doi.org/10.3390/cells11101664.
4. Bachoud-Lévi A-C, Massart R, Rosser A. Cell therapy in Huntington's disease: Taking stock of past studies to move the field forward. Stem Cells 2021;39:144–55. https://doi.org/10.1002/stem.3300.
5. Eskandari N, Boroujeni ME, Abdollahifar MA, Piryaei A, Khodagholi F, Mirbehbahani SH, et al. Transplantation of human dental pulp stem cells compensates for striatal atrophy and modulates neuro-inflammation in 3-nitropropionic acid rat model of Huntington's disease. Neurosci Res 2021;170:133–44. https://doi.org/https://doi.org/10.1016/j.neures.2020.12.002.
6. Sanchez-Diaz M, Quiñones-Vico MI, Sanabria de la Torre R, Montero-Vílchez T, Sierra-Sánchez A, Molina-Leyva A, et al. Biodistribution of Mesenchymal Stromal Cells after Administration in Animal Models and Humans: A Systematic Review. J Clin Med 2021;10:2925. https://doi.org/10.3390/jcm10132925.
7. Costa VR, Araldi RP, Vigerelli H, D'Ámelio F, Mendes TB, Gonzaga V, et al. Exosomes in the tumor microenvironment: From biology to clinical applications. Cells 2021;10:2617. https://doi.org/10.3390/cells10102617.
8. Kerkis I, Kerkis A, Dozortsev D, Stukart-Parsons GC, Gomes Massironi SM, Pereira L V., et al. Isolation and characterization of a population of immature dental pulp stem cells expressing OCT-4 and other embryonic stem cell markers. Cells Tissues Organs 2006;184:105–16. https://doi.org/10.1159/000099617.
9. Lizier NF, Kerkis A, Gomes CM, Hebling J, Oliveira CF, Caplan AI, et al. Scaling-up of dental pulp stem cells isolated from multiple niches. PLoS One 2012;7:e39885. https://doi.org/10.1371/journal.

pone.0039885.

10. Kerkis I, Valverde Wenceslau C, Pinheiro Araldi R. Stem Cells from Dental Pulp of Deciduous Teeth: Twenty Years of Experience. Recent Updat. Mesenchymal Stem Cells, IntechOpen; 2024. https://doi.org/10.5772/intechopen.1003850.
11. Gonzaga VF, Wenceslau CV, Vieira DP, Policiquio B de O, Khalil C, Araldi RP, et al. Therapeutic Potential of Human Immature Dental Pulp Stem Cells Observed in Mouse Model for Acquired Aplastic Anemia. Cells 2022;11:2252. https://doi.org/10.3390/cells11142252.
12. Macedo J, Pagani E, Wenceslau C, Ferrara L, Kerkis I. A pahse I clinical trial on intravenous administration of immature human dental pulp stem cells (NestaCell) to Huntington's disease patients. Cytotherapy 2021;23:1. https://doi.org/10.1016/j.jcyt.2021.02.008.
13. Araldi RP, Ramos AT, Alievi AL, Policíquio B, Teixei MR, Mendes TB, et al. NestaCell® promotes motor, cognitive and neuropsychiatric functions amelioration and dopaminergic neurons restoration in a preclinical model of Parkinson's disease. Cytotherapy 2022;24:S3. https://doi.org/10.1016/S1465-3249(22)00849-0.
14. Araldi RP, Prezoto BC, Gonzaga V, Policiquio B, Mendes TB, D'Amélio F, et al. Advanced cell therapy with low tissue factor loaded product NestaCell® does not confer thrombogenic risk for critically ill COVID-19 heparin-treated patients. Biomed Pharmacother 2022:112920. https://doi.org/10.1016/j.biopha.2022.112920.
15. Araldi RP, Viana M, Colozza-gama GA. Unique transcriptional signatures observed in stem cells from the dental pulp of deciduous teeth produced on a large scale. Pharmacologia 2023;14:72–95.
16. Suzuki S, Namiki J, Shibata S, Mastuzaki Y, Okano H. The neural stem/progenitor cell marker nestin is expressed in proliferative endothelial cells, but not in mature vasculature. J Histochem Cytochem 2010;58:721–30. https://doi.org/10.1369/jhc.2010.955609.
17. Kerkis I, Caplan AI. Stem cells in dental pulp of deciduous teeth. Tissue Eng Part B Rev 2012;18:129–38. https://doi.org/10.1089/ten.teb.2011.0327.
18. Kerkis I, Wenceslau CV, Souza DM, Mambelli-Lisboa NC, Ynoue LH, Araldi RP, et al. Preclincal assessment of NestaCell® in Huntigton's disease 3-NP rat model demonstrates restoration of BDNF, DARPP32, and D2R expression following intravenous single versus multiple injections. Cytotherapy 2022;24:S5. https://doi.org/10.1016/S1465-3249(22)00855-6.
19. Choudhery MS, Mahmood R, Harris DT, Ahmad FJ. Minimum criteria for defining induced mesenchymal stem cells. Cell Biol Int 2022;46:986–9. https://doi.org/10.1002/cbin.11790.
20. Dominici M, Le Blanc K, Mueller I, Slaper-Cortenbach I, Marini F, Krause D, et al. Minimal criteria for defining multipotent mesenchymal stromal cells. The International Society for Cellular Therapy position statement. Cytotherapy 2006;8:315–7. https://doi.org/10.1080/14653240600855905.
21. Silva JM, Araldi RP, Colozza-Gama GA, Pagani E, Sid A, Valverde CW, et al. Human immature dental pulp stem cells did not graft into a preexisting human lung adenocarcinoma. Case Rep Oncol 2022;15:413–22. https://doi.org/10.1159/000523896
22. Kamiyama Y, Naritomi Y, Moriya Y, Yamamoto S, Kitahashi T, Maekawa T, et al. Biodistribution studies for cell therapy products: Current status and issues. Regen Ther 2021;18:202–16. https://doi.org/10.1016/j.reth.2021.06.005.
23. Beal MF, Brouillet E, Jenkins BG, Ferrante RJ, Kowall NW, Miller JM, et al. Neurochemical and histologic characterization of striatal excitotoxic lesions produced by the mitochondrial toxin 3-nitropropionic acid. J Neurosci 1993;13:4181 LP – 4192. https://doi.org/10.1523/JNEUROSCI.13-10-04181.1993.
24. Borlongan C. 3-Nitropropionic acid animal model and Huntington' s disease. Neurosci Biobehav Rev 1997;21:289–93. https://doi.org/10.1016/S0149-7634(96)00027-9.
25. Vis, Verbeek, de Waal, ten Donkelaar, Kremer. 3-Nitropropionic acid induces a spectrum of Huntington's disease-like neuropathology in rat striatum. Neuropathol Appl Neurobiol 1999;25:513–21. https://doi.org/10.1046/j.1365-2990.1999.00212.x.
26. Colle D, Santos DB, Moreira ELG, Hartwig JM, dos Santos AA, Zimmermann LT, et al. Probucol increases striatal glutathione peroxidase activity and protects against 3-nitropropionic acid-induced pro-oxidative damage in rats. PLoS One 2013;8:e67658. https://doi.org/10.1371/journal.pone.0067658.
27. Krachler M, Radner H, Irgolic KJ. Microwave digestion methods for the determination of trace elements in brain and liver samples by inductively coupled plasma mass spectrometry. Anal Bioanal Chem 1996;355:120–8. https://doi.org/10.1007/s0021663550120.
28. Takahashi S, Takahashi I, Sato H, Kubota Y, Yoshida S, Muramatsu Y. Determination of major and trace elements in the liver of Wistar rats by inductively coupled plasma-atomic emission spectrometry and mass spectrometry. Lab Anim 2000;34:97–105. https://doi.org/10.1258/002367700780577966.
29. Barbash IM, Chouraqui P, Baron J, Feinberg MS, Etzion S, Tessone A, et al. Systemic delivery of bone marrow–derived mesenchymal stem cells to the infarcted myocardium. Circulation 2003;108:863–8. https://doi.org/10.1161/01.CIR.0000084828.50310.6A.
30. Fischer UM, Harting MT, Jimenez F, Monzon-Posadas WO, Xue H, Savitz SI, et al. Pulmonary oassage is a major obstacle for intravenous stem cell delivery: The pulmonary first-pass effect. Stem Cells Dev 2009;18:683–92. https://doi.org/10.1089/scd.2008.0253.
31. Gao J, Dennis JE, Muzic RF, Lundberg M, Caplan AI. The dynamic in vivo distribution of bone marrow-derived mesenchymal stem cells after infusion. Cells Tissues Organs 2001;169:12–20. https://doi.org/10.1159/000047856.
32. Eggenhofer E, Benseler V, Kroemer A, Popp FC, Geissler EK, Schlitt HJ, et al. Mesenchymal stem cells are short-lived and do not migrate beyond the lungs after intravenous infusion. Front Immunol 2012;3. https://doi.org/10.3389/fimmu.2012.00297.
33. Horie M, Choi H, Lee RH, Reger RL, Ylostalo J, Muneta T, et al. Intra-articular injection of human mesenchymal stem cells (MSCs) promote rat meniscal regeneration by being activated to express Indian hedgehog that enhances expression of type II collagen. Osteoarthr Cartil 2012;20:1197–207. https://doi.org/10.1016/j.joca.2012.06.002.
34. Horie S, Gonzalez HE, Laffey JG, Masterson CH. Cell therapy in acute respiratory distress syndrome. J Thorac Dis 2018;10:5607–20. https://doi.org/10.21037/jtd.2018.08.28.
35. Koç ON, Gerson SL, Cooper BW, Dyhouse SM, Haynesworth SE, Caplan AI, et al. Rapid Hematopoietic Recovery After Coinfusion of Autologous-Blood Stem Cells and Culture-Expanded Marrow Mesenchymal Stem Cells in Advanced Breast Cancer Patients Receiving High-Dose Chemotherapy. J Clin Oncol 2000;18:307–307. https://doi.org/10.1200/JCO.2000.18.2.307.
36. Gholamrezanezhad A, Mirpour S, Bagheri M, Mohamadnejad M, Alimoghaddam K, Abdolahzadeh L, et al. In vivo tracking of 111In-oxine labeled mesenchymal stem cells following infusion in patients with advanced cirrhosis. Nucl Med Biol 2011;38:961–7. https://doi.org/10.1016/j.nucmedbio.2011.03.008.
37. Wu J, Sun Z, Hong-Shuo S, Wu J, Weisel RD, Keating A, et al. Intravenously administered bone marrow cells migrate to damaged brain tissue and improve neural function in ischemic rats. Cell Transplant 2018;16:993–1005.
38. Yilmaz G, Vital S, Yilmaz CE, Stokes KY, Alexander JS, Granger DN. Selectin-Mediated Recruitment of Bone Marrow Stromal Cells in the Postischemic Cerebral Microvasculature. Stroke 2011;42:806–11. https://doi.org/10.1161/STROKEAHA.110.597088.
39. Constantin G, Marconi S, Rossi B, Angiari S, Calderan L, Anghileri E, et al. Adipose-Derived Mesenchymal Stem Cells Ameliorate

Chronic Experimental Autoimmune Encephalomyelitis. Stem Cells 2009;27:2624–35. https://doi.org/10.1002/stem.194.

40. Leibacher J, Henschler R. Biodistribution, migration and homing of systemically applied mesenchymal stem/stromal cells. Stem Cell Res Ther 2016;7:7. https://doi.org/10.1186/s13287-015-0271-2.
41. Kim S, Lee S, Jung H-S, Kim S-Y, Shin S-J, Kang MK, et al. Evaluation of the Biodistribution of Human Dental Pulp Stem Cells Transplanted into Mice. J Endod 2018;44:592–8. https://doi.org/10.1016/j.joen.2017.12.007.
42. Satani N, Cai C, Giridhar K, McGhiey D, George S, Parsha K, et al. World-Wide Efficacy of Bone Marrow Derived Mesenchymal Stromal Cells in Preclinical Ischemic Stroke Models: Systematic Review and Meta-Analysis. Front Neurol 2019;10. https://doi.org/10.3389/fneur.2019.00405.

Appendix A

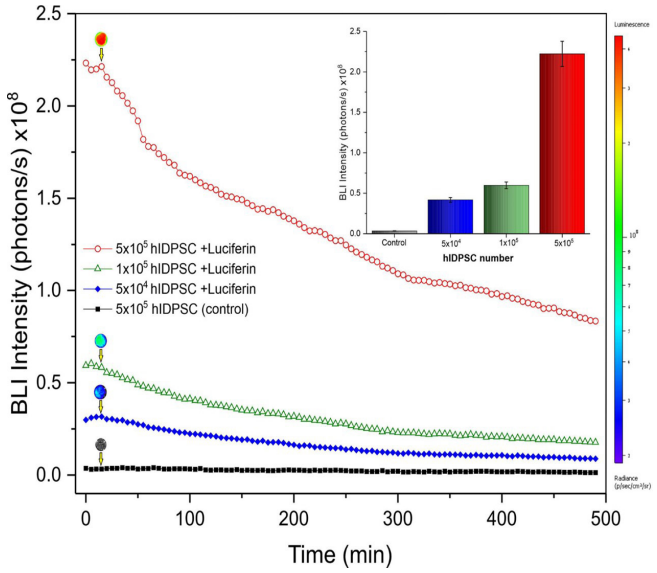

Figure A1: *Expression of the BLM signal as a function of the number of Luc-hIDPSC over 480 minutes, thus indicating peak intensity 5 minutes after D- luciferin administration. Inset Quantification of peak BLI signal intensities in chest at Luc-hIDPSC concentrations of 5 X 104, 1 X 105, and 5 X 105 detected 5 minutes after D- luciferin administration.*

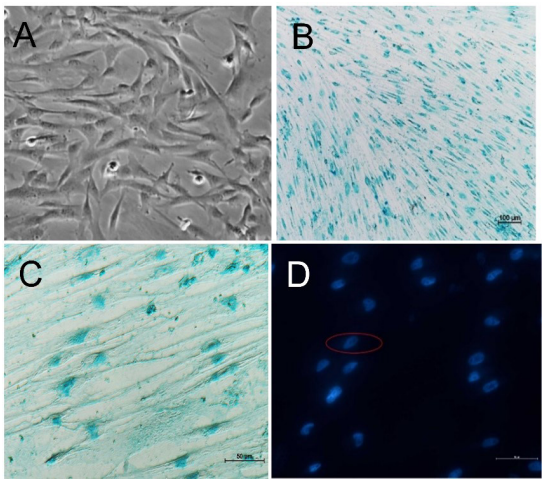

Figure A2: *Brightfield microscopy of MNP-hIDPSC (NP750) (A). Blue staining shows the presence of NP750 at various magnifications: A (20x), B (10x), C (40x). (D) The fluorescent labeling of cell nuclei by DAPI (4',6-diamidino-2-phenylindole); 40 µg Fe/mL were used for labeling (40x).*

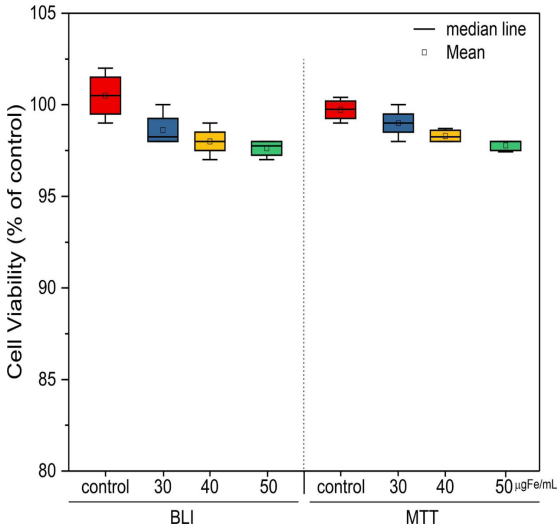

Figure A3: *Evaluation of cell viability by BLM and MTT techniques, after 48 hours of labeling the hIDPSC with MNP at concentrations of 30, 40 and 50 µg Fe/mL.*

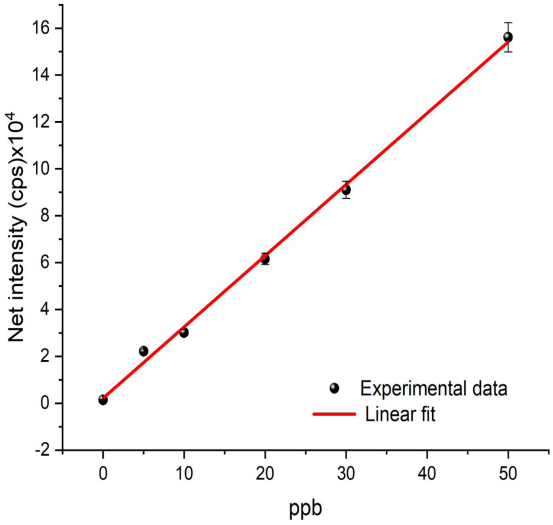

Figure A4: *Calibration curve produced at concentrations 0.5, 10, 20, 30 and 50 ngFe/mL from the standard MNP sample.*

Citation: *Cristiane Wenceslau Valverde. Assessing the Biodistribution of Human Immature Dental Pulp Stem Cells (NestaCell®) via Intravenous Administration in Mice: A Non-Clinical Investigation . Jour of Clin Cas Rep, Med Imag and Heal Sci 8(4)-2024.
DOI: 10.55920/JCRMHS.2024.08.001356

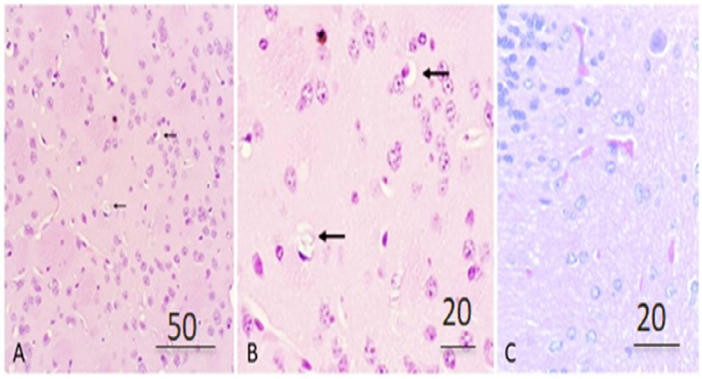

Figure A5: *Neuronal vacuolization in the striatum found in the 6-week-old female C57BL/6. In (B) high magnification in (A), and, on the right: normal brain, without histopathological changes (control animal). Arrows in (A, B) indicate neuronal vacuolization. (C) – Negative control, striatum of the animal not treated with 3-NPA.*

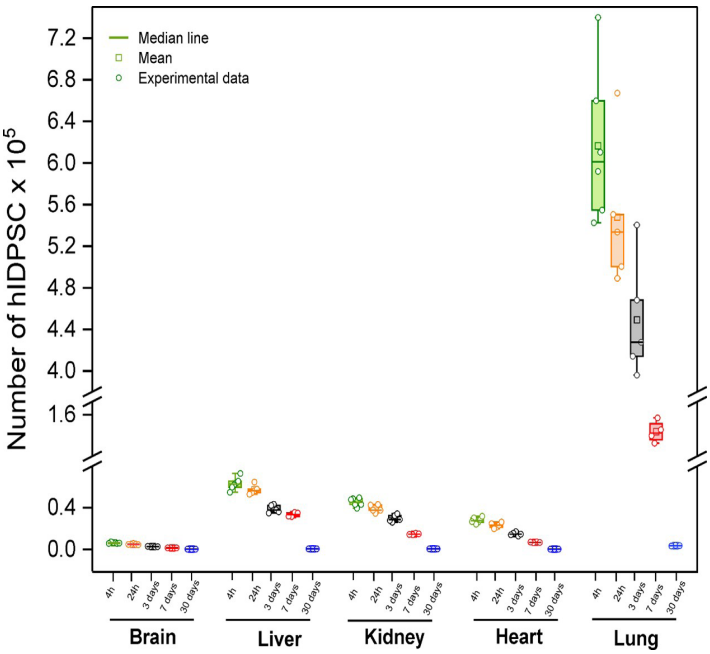

Figure A6: *Box plot of the biodistribution of MNP-hIDPSC in the brain, liver, kidney, heart and lung and quantification of cells by the ICP-MS technique at 4, 24 and 72 hours, 7 and 30 days.*

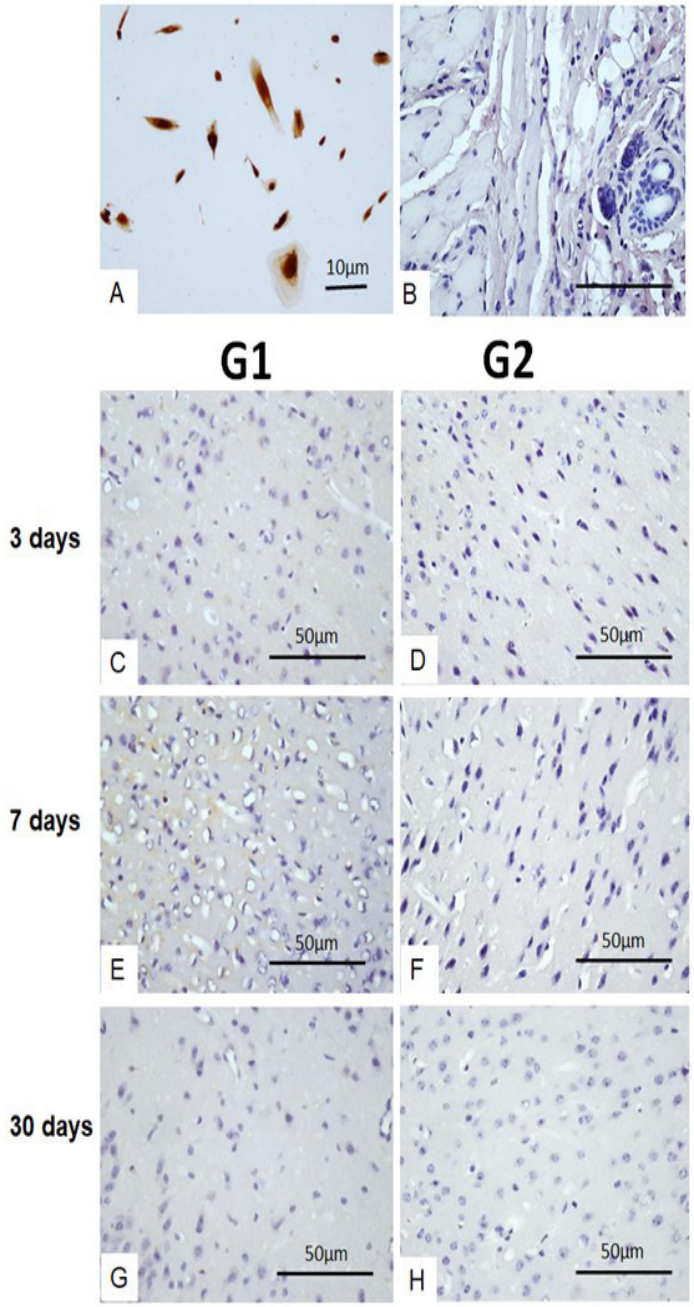

Figure A7: *Demonstrates respective controls to anti-human mitochondrial (hAMA) antibody. (A) Shows positive hAMA staining in hIDPSCs. (B) The mouse epidermis control for non-specific binding of the secondary anti-rabbit anti-body, which demonstrates the absence of staining, when primary antibody was omitted. (G-H) No hAMA immunostaining observed in the mouse cortex on day 3 (C, D), on day 7 (E, F) and on day 30 (G, H), respectively, in control groups G1 and G2, which did not receive hIDPSC administration. Scale bar: (A) = 10µm, (B – H) = 100µm. The nuclei were stained with hematoxylin and eosin (HE).*

Citation: *Cristiane Wenceslau Valverde. Assessing the Biodistribution of Human Immature Dental Pulp Stem Cells (NestaCell®) via Intravenous Administration in Mice: A Non-Clinical Investigation . Jour of Clin Cas Rep, Med Imag and Heal Sci 8(4)-2024.

DOI: 10.55920/JCRMHS.2024.08.001356